Ceramics International 49 (2023) 9826–9838

Contents lists available at ScienceDirect

Ceramics International

journal homepage: www.elsevier.com/locate/ceramint

Optimization of the nucleating agent content for the obtaining of transparent fluormica glass-ceramics

Khalissa Ariane [a], Aitana Tamayo [b,*], Abdellah Chorfa [a,c], Fausto Rubio [b], Juan Rubio [b,*]

[a] Institute of Optics and Precision Mechanics, Ferhat Abbas University Setif 1, Setif, Algeria
[b] Ceramics and Glass Institute, CSIC, Madrid, Spain
[c] Laboratory of Applied Optics, IOMP, Ferhat Abbas University Setif 1, Setif, Algeria

ARTICLE INFO

Keywords:
Glass-ceramic
Crystallization kinetics
P_2O_5
Transmittance
Mica

ABSTRACT

The crystallization behaviours, mechanical and optical properties of fluormica glass-ceramic system without and with P2O5 as nucleating agent are studied. The crystallization mechanism of fluor-phlogopite ($KMg_3(Si_3AlO_{10})F_2$) without P_2O_5 oxide represented one-dimensional surface crystallization with a fixed number of nuclei, and with the addition of P_2O_5, the mechanism tends to two-dimensional bulk crystallization with a constant nucleation rate being the most predominant phase, forsterite crystals (Mg_2SiO_4). The base glasses had the spinodal phase separation, which coarsened considerably by increasing P_2O_5 content. P_2O_5 had a strong influence on the microstructure and morphology of this type of glass-ceramic. The addition of small amount of P_2O_5 (1.0 mol%) to these glass-ceramic changed the microstructure from dendritic growth having *leaf-like* feature to a *flower-like* morphology of the crystal phase. Glass-ceramic without P_2O_5 produces yellowish to colourless transparent glass-ceramic, and with the incorporation of the P_2O_5 (1.0 mol%), which has been found the optimum to obtain transparent glass-ceramics, the transmittance is still about 85%. As the P_2O_5 content increased to 3.0 mol%, besides fluor-phlogopite mica, forsterite also precipitates, the size of the crystals increase, their distributions turned to be broad due to the change of the crystallization mechanism and the transparency of glass-ceramic consequently decreases.

1. Introduction

Glass-ceramics (GC) are a kind of polycrystalline material formed by controlled crystallization of the parent glasses. They demonstrate the ability to combine various remarkable properties in one material based on variability in chemical composition, microstructure and heat-treatment conditions [1]. Their properties could be inherent to the glass itself, or could be a result of modifications in structure and microstructure arising from processing techniques [2]. An important group of these materials are the mica-containing GC which received wider attention due to their high machinability and thermal shock resistance [3–5]. The most common compositions of mica GC lie in the system SiO_2–B_2O_3-$A1_2O_3$–MgO–K_2O–F [6]. Depending on the base glass compositions several mica phases can precipitate: fluorophlogopite mica ($KMg_3AlSi_3O_{10}F_2$), tetrasilicic mica ($KMg_{2.5}Si_4O_{10}F_2$) [5,7–9], Li-phlogopite ($LiMg_3AlSi_3O_{10}F_2$) [10,11], calcium-mica ($Ca_{0.5}Mg_3(AlSi_3O_{10})F_2$) [12], and barium-calcium-mica [$BaCa_{0.5}Mg_3AlSi_3O_{10}F_2$] [13]. Over controlled heat-treatment, alumino-silicate glasses of the K–Mg–Al–Si–O–F system are converted to GC containing fluorophlogopite mica ($KMg_3AlSi_3O_{10}F_2$) through a nucleation process [5,7]. Crystallization process is generally affected by nucleating agents, which either accumulate in a specific microphase of the phase separated base glass or support the phase separation.

Light scattering arising from the difference in refractive indices of crystals and the surrounding glass phase is present in any GC material. According to the Rayleigh–Gans scattering model, the scattering loss is proportional to the refraction index of the crystal phase and the difference with the surrounding glass, to the crystallite density, their radius and volume and the incident light wavelength [14]. The scattering loss (turbidity), is extremely sensitive to the size of the crystals and the difference in refractive index. To achieve transparency in GC several strategies can be followed: by reducing the size of the crystalline phases below the wavelength, by growing crystals with anisotropic refractive index (birefringent crystals) or achieving a match in refractive index with residual glass, a condition which is easy to meet for GCs in which glassy phase and crystalline phase have nearly same composition [14].

* Corresponding authors. Ceramics and Glass Institute, CSIC, Kelsen 5, 28049, Madrid, Spain.
E-mail addresses: aitanath@icv.csic.es (A. Tamayo), jrubio@icv.csic.es (J. Rubio).

https://doi.org/10.1016/j.ceramint.2022.11.156
Received 27 July 2022; Received in revised form 19 October 2022; Accepted 12 November 2022
Available online 15 November 2022

Thus, due to the growth of crystalline phases, GC can easily loose the transparency. To avoid that, both the nucleation and crystal growth rates should be carefully controlled to prevent from overgrowth and coarsening of crystals. Ensuring crystal sizes below 100 nm is a prerequisite for achieving high transparency of GC. As an example, Ghasemzadeh et al. [15] prepared transparent glass-ceramic from $18MgO–38SiO_2–15Al_2O_3–8K_2O–6B_2O_3–9LiF–6TiO_2$ by controlled crystallization of the parent glass at 643 °C for 2 h. They observed that the glass-ceramic can remain transparent upon precipitation of nano sized grains but they will turn into opaque when large grains appear.

Mg^{2+} is an important component of the mica structure since it octahedrically accommodates between the corner-shared tetrahedral network. With the increase of Mg content, there occurs a tendency to phase separation since the Mg^{2+} ions helps balancing the $[AlO_4]^-$ tetrahedron. Because of the excellent compatibility of the $[SiO_4]$ tetrahedron and the $[AlO_4]_2Mg$ complexes, the precipitation of mica units are thus enhanced [16]. This strategy of nanophase separation followed by the formation of crystalline phases that contain nucleating oxides has been widely used to prepare GC. In the work of Fathi and Johnson [17], it is demonstrated that the high ionic field of TiO_2 enhances the phase separation thus improving the heterogeneous nucleation of the crystals within the glassy network [17]. By incorporating some other nucleating agents to the parent glass such as TiO_2, ZrO_2, MoO_3, P_2O_5, and F the thermodynamics and kinetics of the nucleation process can be further modified [18].

It is known that fluorine ions are insoluble in silicate melts also leading to phase separation [19], and also, they will promote bulk nucleation and three-dimensional crystal growth of the principal crystalline phase [20]. As Radonjić and Nicolić [20] reported, in glasses of the MAS system (MAS: $MgO-A1_2O_3–SiO_2$), it was proved that the fluorine ions significantly influenced the crystallization kinetics as well as crystal morphology. Similarly, Taruta et al. [21] fabricated transparent GC from the $Li_{(1+x)}Mg_3AlSi_{3(1+x)}O_{10+6.5x}F_2$ system in which large quantities of mica crystals were obtained when the nucleating agent MgF_2 was added at amounts between 9 and 13% and by increasing the amount of this agent, the crystallization of mica occurs into a continuous glass phase and the parent glass loses its transparency due to the formation of a coarser spinodal phase separation. GC with MgF_2 as the source of fluorine exhibits uniform bulk crystallization but on contrary, if NaF is incorporated as nucleating agent only surface crystallization occurs [22].

Some other ions could act as nucleating agents to modify the crystallization process for the production of fine-grained fluormica glass-ceramics by controlled crystallization [23,24]. As an example, through the addition of 3–6% PbO and P2O5 to the base glasses, it occurs a change in the mica crystals morphology from platelet to spherical shapes attributed to a decrease in the crystallite growth rate [25]. Besides, mica crystallization was affected by the addition of P_2O_5 in the sense that, according to Mirsaneh et al. [26], the addition of ⩾4 mol% P_2O_5 induces a liquid-liquid type phase separation of the glass thus producing a silica glass matrix deficient in network modifiers. This phase separation is attributed to the high field strength of Si^{+4} and P^{5+} atoms. The former possess a higher field strength thus induces its association to the alkaline atoms (Ca or Mg) and consequently, the precipitation of the silica-rich mica phase is less likely to occur. In the present work, we focus on the preparation of transparent $K_2O–MgO–Al_2O_3–B_2O_3–SiO_2–MgF_2$ GC where the crystallization products and kinetics are tailored through the addition of P_2O_5 as nucleating agent to optimize the amount of nucleating agent for the maintaining of the transparency of the obtained materials.

2. Experimental

2.1. Preparation of materials and procedures

The system $K_2O–MgO–Al_2O_3–B_2O_3–SiO_2$ plus MgF_2 and P_2O_5 as nucleating agent has been studied in the present work. The starting chemicals were SiO_2, Al_2O_3, $MgCO_3$, MgF_2, K_2CO_3 and H_3BO_3, all of them chemical grade (Panreac). The nominal composition of the original glass (MP0) is given in Table 1. P_2O_5 (purity>98%) was added to MP0 in 1.0 (MP1), 2.0 (MP2) and 3.0 (MP3) mol%. Each 100 g batch was well mixed, calcined in a platinum crucible using an electric furnace for 3 h at a temperature of 900 °C (heating rate of 10 °C/min), and then melted at about 1600 °C (10 °C/min) and held for 3 h till complete homogenization. Then, the molten charge was poured to a preheated copper molds. The as-prepared samples were further annealed at 550 °C (10 °C/min) for 4 h and cooled to room temperature (2 °C/min) in a programmed manner with the aim to eliminate thermal residual stresses. The GC samples were prepared by annealing the base glasses for 3 h at 750 °C. The composition of all the base glasses, obtained by ICP-OES spectrometry (Iris Advantage, Thermo Jarrel Ash) and X-ray fluorescence (Philips, Magic Pro) is also provided in Table 1 (values given in wt%).

2.2. Characterization

Powdered samples were analysed by X-ray diffraction (XRD, Bruker D8 Advance) at room temperature in the 2θ range 10–70° (step size 0.05, 15s) and the developed crystalline phases were identified by JCPDS numbers (ICDD-PDF database). The Fourier-Transform infrared absorption spectra were recorded using a Fourier transform infrared spectrometer (Alpha FTIR, Bruker, Germany) at room temperature, in the range 4000−400 cm^{-1}, using the KBr pellet technique, with a resolution 2 nm. The spectra were averaged from 32 scans. Room temperature Raman spectra were recorded using a Raman spectrometer (Renishaw, UK) with a 20 mW Argon ion laser source at an excitation wavelength of 514 nm. All measurements were made in a back scattering geometry, using a 50 × microscope objective lens (0.25 μm lateral resolution). The spectra were averaged over 50 scans. Crystallization kinetic parameters were analysed by differential thermal analysis (DTA, TA Instruments, SDT Q600, USA) using glass powders sieved below 50 μm and heated from 25 to 1300 °C at different heating rates (5, 10, 15 and 20 °C.min^{-1}) in air atmosphere. The error in the determination of the characteristic temperatures is estimated to be ±2 °C. To study the structural and microstructural changes occurring during the heat-treatment, glass samples containing the different amounts of nucleating agent were thermally treated at 700, 750, 800, 850, 900 and 950 °C for 1 h. Hot stage microscopy characterization was performed in a HSM, EM201 Leica instrument equipped with a CCD camera and by analysis of the photographs taken during the HSM experiment. The dilatometer Bahr Thermo Analyzer DIL 801 L, Hüllhorst, Germany working in dry air at a heating rate of 5 °C/min in the range of 25–1000 °C was used for coefficient of thermal expansion (CTE) determinations. For this, sample pieces of 5 × 5x10 mm^3 were used with Al_2O_3 as reference material. Fractured surfaces were etched, with approximately 3.0% HF solution for 15 s to delineate prominent features, then coated with a thin layer of gold for being observed in a field-emission type scanning electron microscopy (FESEM, Hitachi S4700, Tokyo, Japan) operating at 30 kV. The elastic modulus and hardness values of the materials were evaluated using nanoindentation technique (XP Nanoindenter, MTS, Oak Ridge, USA). These tests were performed with a Berkovich indenter continuously registering and with high precision the load (50 mN) and displacement of the indenter during the test. The optical transmission spectra of base glasses and GC were measured with an UV spectrometer (UV–Vis, PerkinElmer Lambda 950) in the wavelength range of 300–1100 nm at room temperature. The refractive indexes (n_D) of the materials were determined through an Abbe refractometer (ATAGO, model DR-A1) with a spectral line of sodium (589.3 nm). Ten measurements were made on each sample and averaged at the ambient temperature of 22 ± 02 °C.

Table 1
Nominal composition (mol.%) of oxides used to prepare the parent glass MP0 and actual composition (wt%) of all the prepared glasses.

MP0 (nominal)	SiO_2	Al_2O_3		K_2CO_3	MgO	B_2O_3		MgF_2	P_2O_5
	44	9		6	29	2		10	00
% oxides	SiO_2	Al_2O_3	K_2O	MgO	B_2O_3	CaO	Fe_2O_3	F	P_2O_5
MP0	39.78	8.47	5.10	33.60	1.40	0.56	<0.03	11.07	0
MP1	40.12	9.65	4.75	33.31	1.37	0.56	0.04	9.42	0.79
MP2	39.69	8.58	4.73	33.89	1.28	0.56	0.05	9.68	1.57
MP3	39.40	8.33	4.80	33.48	1.29	0.56	0.04	9.77	2.34

3. Results and discussion

Table 1 presents the composition of all the base glasses in terms of the oxide percentages. As expected, all the glasses present similar compositions since the only modification is the amount of P_2O_5 included. It is however observed that the maximum amount of fluorine is encountered in the MP0 glass (i.e. no P_2O_5 added) thus, the presence of the nucleating agent at any concentration will cause a decrease in the fluorine content. It should be noticed that although no Fe or Ca was included, some traces of these oxides were present in the final composition of the base glasses. The reason for the appearance of these two elements is the probable presence of Fe_2O_3 in quartz and $CaCO_3$ in the K_2CO_3 used to prepare the glasses (raw materials were chemical grade, some impurities can still be present).

3.1. Evolution of the crystalline phases

3.1.1. XRD

The XRD patterns of all the base glasses (Fig. 1 a) are characteristic of amorphous materials, since no clear reflections on the diffractograms are appreciated and just the occurrence of two broad halos around $2\theta = 17°$ and 28° might be an indicative of some degree of phase separation, as suggested by other authors [27]. As shown in Fig. 1 b, in MP3 samples, those containing the maximum amount of the nucleating agent P_2O_5, the fluor-phlogopite (1 M, $KMg_3(Si_3AlO_{10})F_2$, JCPDS No. 00-010-0494) appeared at temperatures as low as 750 °C though the peaks in the XRD pattern were still small. Early investigations [19] proved that fluor-phlogopite is the main crystalline phase which should appear after heat-treatment at 800 °C the mica-containing containing glass ceramics. By increasing the temperature (Fig. 1 c), the growth of fluor-phlogopite is more evident and, as the P_2O_5 content increases in the materials, forsterite (Mg_2SiO_4, JCPDS No. 00-004-0769) appeared as well. With increasing the heating temperature, fluor-phlogopite peaks become obviously stronger and, at the same time, some other weak diffraction peaks of forsterite are observed. It is then noticed that the diffraction peaks attributed to forsterite are more intense in the samples containing the highest P_2O_5 content, and, contrarily, the lowest P_2O_5 amount implies an enhanced crystallization of fluor-phlogopite. It is also noticed that at 850 and 950 °C (Fig. 1c and d) and at the lowest P_2O_5 contents, an additional diffraction peak appeared at about $2\theta = 28°$

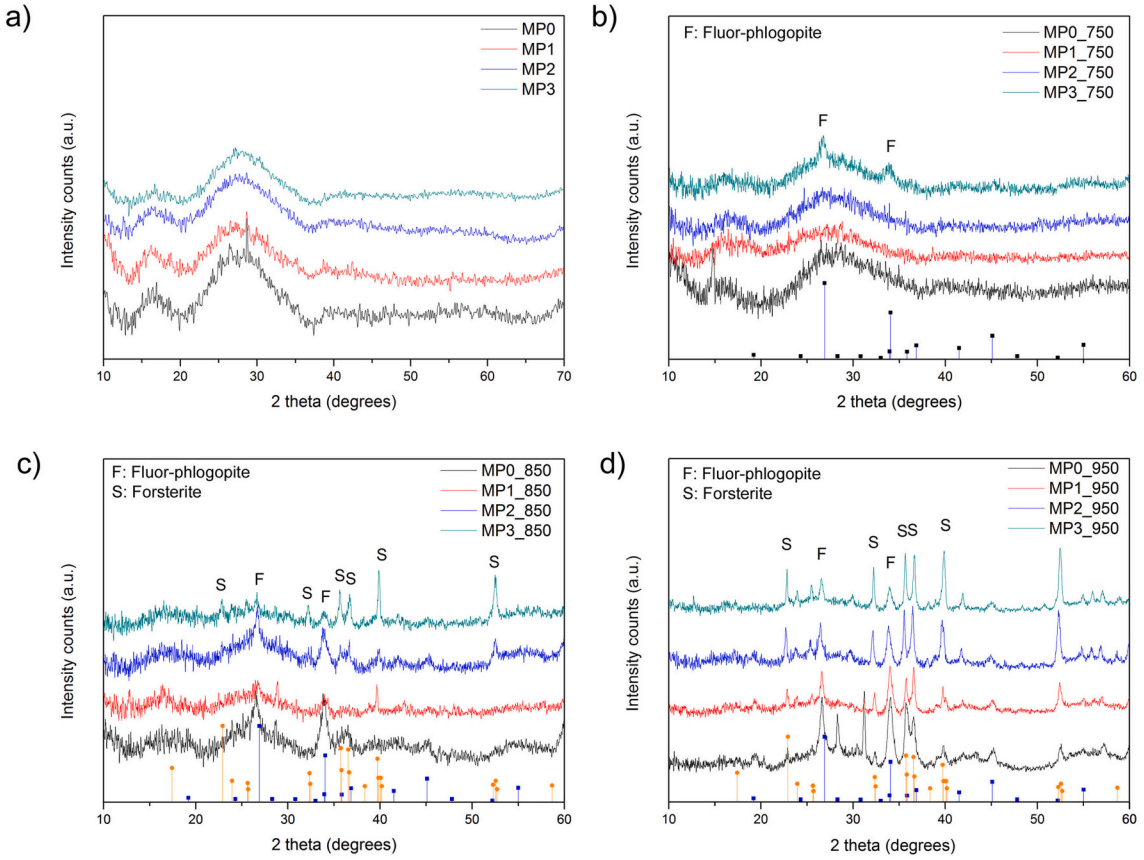

Fig. 1. X-ray diffraction patterns of the samples MP0, MP, MP2 and MP3 treated at a) as-prepared, b) 750, c) 850, and d) 950 °C. S: Forsterite, syn, F: Fluor-phlogopite, 1 M.

which is tentatively attributed to phlogopite.

3.1.2. Thermal properties

The differential thermal analysis thermographs at a heating rate of 10 °C/min of the four studied glasses are shown in Fig. 2. Table 2 shows the thermal parameters from the DTA analysis. From Fig. 2 and Table 2, all curves generally exhibit one endothermic peak and two exothermic peaks corresponding to the glass transition temperature, T_g, and onset crystallization temperatures, T_{c1} and T_{c2}, respectively. The characteristic temperatures were taken as the maximum of the peak (in the case of the exothermic events) or its minimum (in the case of the endothermic events) and by assuming a mixed Gaussian−Lorentzian (50%–50%) shape. The T_g values were determined to be approximately at 660 °C for MP0 and then increased slightly to 667 °C when P_2O_5 was added to the system at amounts up to 1.0 mol%. A further increase in the content of P_2O_5 (2.0 and 3.0 mol%) caused a marked decrease of this temperature, since P_2O_5 lowers the glass transition. This may associated with a lower glass viscosity.

In Fig. 2 d, there are emphasized in colour the onset crystallization temperatures, T_{c1} and T_{c2}. It is also observed multiple bands in the DTA which are attributable to the maximum crystallization temperatures, T_m, and the release of the Gibbs free energy because of the formation of the GC.

The dilatometric curves (Fig. 3 a) allow determining the glass transition temperature for the base glasses. The T_g values of the base glasses determined from the dilatometric curves are collected in Table 2. T_g is frequently used to characterize the glass-forming ability of the glasses and it is often taken to be equal to the temperature at which the glasses possess a specific viscosity (10^{13} Pa), so it is important to accurately determine this temperature. As shown in Table 2, although the trends are similar, slight differences are encountered when determining the T_g by DTA and dilatometry, especially at the highest content of the nucleating agent P_2O_5. According to Mazurin [28], the different relaxation times of the structure affect the viscosity and then the viscosity affects the rate of further structural transformations therefore, it should be concluded that the increase of the P_2O_5 content will affect the viscosity parameters as well as the microstructure of the materials.

In the glass ceramics, it is also possible to determine the CTE from the slope of the dilatometric curves in the range 100–500 °C (Fig. 3 b). In MP0, the high CTE is about 10.2 10^{-6} and decreases to 8.5 10^{-6} for the remainder glasses, when P_2O_5 is already present in the materials. This high CTE value is attributed to the high Mg content and the precipitation of forstertite [29,30]. From the first derivative curve, it can be also calculated the volumetric expansivity of the glass ceramics (β), which is also presented in Table 2. The first incorporation of P_2O_5 leads to a drastic decrease of the volumetric expansivity whereas by increasing the P_2O_5 content beyond 2%, the volumetric expansivity remains mostly constant. These results are attributed to the different crystalline phases appearing in the GC.

The thermal behavior of the prepared glasses can be further studied by hot stage microscopy (Fig. 4 a). As expected, the sintering temperature of the glasses decreases with the amount of the P_2O_5 amount. In MP0 glasses, no softening point was detected in the analysed range, whereas for the remainder glasses, it was possible to determine the characteristic temperatures at which the different events (deformation temperature, sphere and half sphere) take place.

Considering the typical viscosity points at which these events should occur, the viscosity-temperature plot has been drawn (Fig. 4 b). Taking into account the T_g values obtained from the DTA analysis (Table 2), the deformation and half sphere temperatures obtained from the HSM plots,

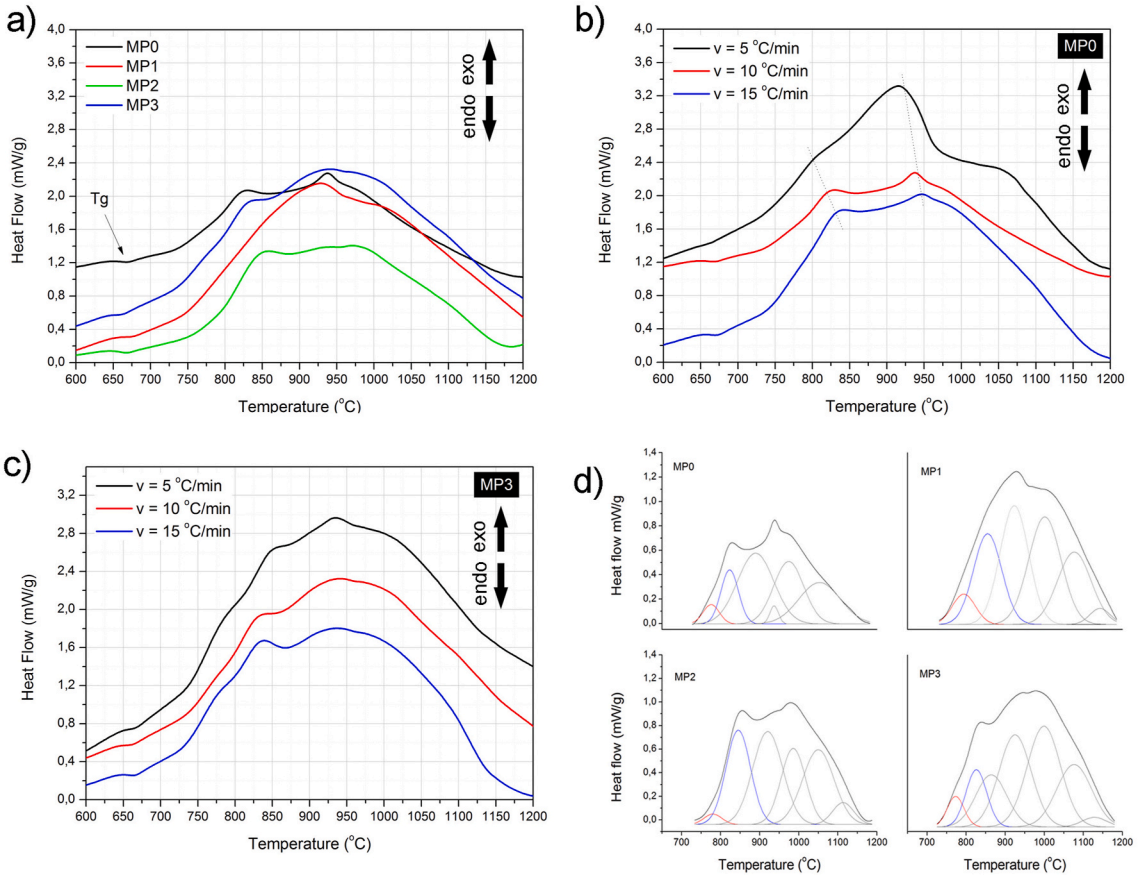

Fig. 2. Differential thermal analysis of the glasses a) heat treated at 10 °C/min, b) the DTA of the MP0 glass heat treated at different heating rates, c) DTA of the MP3 glass heat treated at different heating rates and d) deconvolution of the differential thermogrammes of the glasses heat treated at 10 °C/min.

Table 2
Temperature of the onset crystallization peak, Tc1 and Tc2, glass transition temperature, Tg, (°C) from the DTA curves and dilatometric curves ($(Tg)^{DTA}$ and $(Tg)^{DL}$respectively) and glass stability parameters of base glasses. $\Delta Tx = T_{c1} - T_g$, $S = S = (Tc - Tx)(Tx - Tg)/Tg$, $T_{rg} = T_{rg}(= T_g/T_m)$ CTE is the coefficient of thermal expansion and β is the volumetric expansivity.

	$(T_g)^{DTA}$	$(T_g)^{DL}$	$(T_s)^{DL}$	T_{c1}	T_{c2}	ΔT_x	S	T_{rg}	CTE 10^6	β 10^3
MP0	660	664	720	775	823	55	09.02	0.579	10.2	0.03
MP1	667	667	756	794	855	83	13.12	0.526	8.49	−1.71
MP2	659	650	753	780	845	91	13.10	0.546	8.64	−0.84
MP3	651	642	780	773	826	99	11.60	0.521	8.46	−0.88

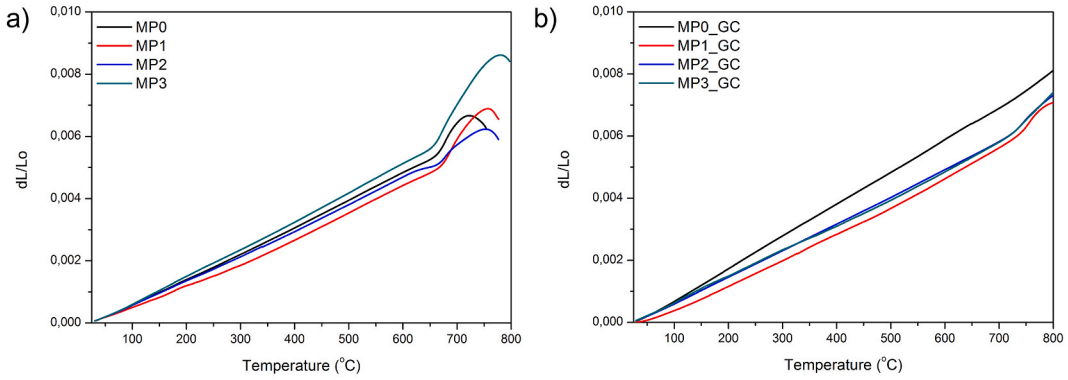

Fig. 3. Dilatometric curves of a) the base glass and b) glass ceramics.

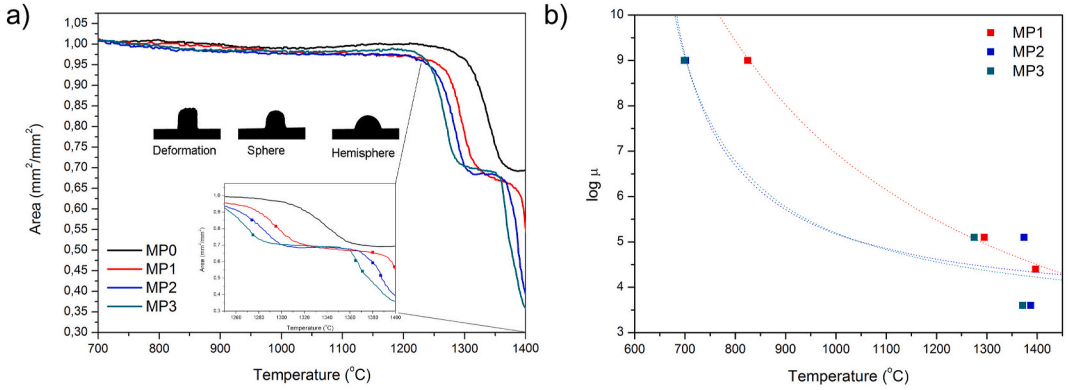

Fig. 4. a) HSM curves of the base glasses and b) viscosity-temperature curves obtained from the characteristic points in the HSM curves and DTA thermograms (dotted lines represent the fitted VFT curves).

the theoretical viscosity curve has been fitted to the Vogel–Fulcher–Tammann equation (plotted in dotted lines) [31]. Form these curves, it can be appreciated the above mentioned decrease in the viscosity when the P_2O_5 increases in the material, as corresponds with the addition of the nucleating agent.

3.1.3. *Crystallization kinetics*

From the DTA scan of the base glasses, it can be seen that the first crystal phase forms at nearly above 770 °C and the second crystal phase at up to 850 °C, that, according to the XRD data they should correspond to the crystallization of fluor-phlogopite and forsterite, respectively. We observe two different crystallization behaviours depending on the P_2O_5 content: for low P_2O_5 content, 1.0 mol%, crystallization peaks are broader and they appear at higher temperature than those without P_2O_5, and for high P_2O_5 content, >1.0 mol%, crystallization peaks shifted gradually to lower temperatures.

The temperatures T_g and T_p are indications of the tendency to maintain the glass structure or crystallize: T_g informs about the structural relaxation occurring in the glass network when the material is subjected to a heating process and T_p informs about the crystallization kinetics of the glass. In the table, it is presented the value $\Delta T_x = T_x - T_g$, where T_x is the onset temperature of the first crystallization peak, that may be considered a reflection of the supercooled liquid region [32]. High ΔT_x values may indicate that the supercooled liquid can exist in a wide temperature range without crystallization and has a high resistance to the nucleation and growth of crystalline phases. A crystallization peak close to the glass transition temperature is usually indicative of unstable glasses. Therefore, the temperature difference ΔT_x is a good indication of thermal stability since the higher the value of this difference, the more the delay in the nucleation process. In our case, ΔT_x varies from 55 to 99 °C with the increase of the P_2O_5 amount, and then, it can be inferred that the higher is the P_2O_5 content, the lower the ability of a glass to crystallize (higher ΔT_x values). Similarly, the index $S = (T_c - T_x)(T_x - T_g)/T_g$, proposed by Saad and Poulain [33] that reflects the resistance to devitrification of a glass when it is heated up is found to increase up with addition of 1.0 mol% P_2O_5, and then showed a decrease with further increase of P_2O_5 content.

The crystallization mechanism for our samples was studied using DTA measurements. Peak positions, T_{c1} and T_{c2}, full-width of the exothermic peak at half-maximum intensity (Δw) and intensities of the

peaks were obtained from a deconvolution procedure of different DTA curves assuming that every peak presents a mixed Gaussian−Lorentzian (50%–50%) shape.

The T_g of different specimens was determined to be comprised between 649 and 673 °C, and shifted to higher temperature with the increase of heating rate. In a similar fashion, the crystallization peaks also generally shift to higher temperatures with the increase of the heating rate from 5 to 20 °C.min^{-1}.

The variation of the onset crystallization peaks T_{c1} and T_{c2} with different DTA heating rates (v) is used to calculate activation energy for crystallization and allows identifying the most plausible crystallization mechanism. In the present work the activation energy of crystallization (E_c) for the different base glasses was determined by using three different methods. The Kissinger [34] equation is one of the most common methods to calculate the crystallization activation energy by plotting the inverse of the onset crystallization temperature, $1/T_c$ versus ln (v/T_c^2). Matusita−Sakka [35] stated that the Kissinger equation must be only used if crystal growth occurs on a fixed number of nuclei and have suggested a modified form of the Kissinger equation as:

$$ln\left(\frac{v^n}{T_c^2}\right) = -m\frac{E_c}{R.T_c} + constant \qquad \text{Equation 2}$$

where m refers to the crystal growth dimensionality and the Avrami parameter n [36,37]:

$$n = \frac{2.5\ R\ T_c^2}{\Delta w\ E_c} \qquad \text{Equation 1}$$

The parameters m and n can take various values: for surface crystallization $n = m = 1$, for bulk crystallization with a constant number of nuclei independent of temperature $n = m$ and, for bulk crystallization with an increasing number of nuclei inversely proportional to the heating rate $n = m + 1$ [35]. The Avrami parameter, $n = 1$ indicates one-dimensional growth (surface crystallization), $n = 2$ indicates two-dimensional crystallization, and $n = 3$ implies three-dimensional growth (bulk crystallization). The DTA curves present two peaks at different heating rates T_{c1} and T_{c2} and the values of E_c for crystallization calculated by the Matusita−Sakka method, the values of Avrami exponent n and the m parameter of the two exothermic peaks are given in Table 3.

As observed in Table 3, the activation energies fall in the range of 170–500 kJ mol^{-1}, which are quite high activation energy values compared to the ones found in Refs. [7,19,38]. In the first crystallization peak, the E_c slightly increases with addition of 1.0 mol% P_2O_5, and then decreases as the P_2O_5 amount increases. On contrary, in the second crystallization peak the E_c values are higher than those found for MP0 glasses except for the material containing the highest amount of P_2O_5. According to the XRD data, the tendency to crystallization of fluor-phlogopite is promoted by small amounts of P_2O_5, however, for the crystallization of forsterite, it is required P_2O_5 contents higher than 3% for the E_c value to decrease.

Using the E_c values, the Avrami constants corresponding to the crystallization mechanism were determined. The values of m in this work are approximately equal to the values of n, i.e. the nuclei formed in the first heat-treatment before the thermal analysis run are dominant (crystallization occurs on a fixed number of nuclei). The crystallization index m is related to the dimensionality of the crystal growth, $m = 1$ indicates one-dimensional growth (surface crystallization), and $m = 2$ implies two-dimensional growth (bulk crystallization). A surface crystallization mechanism occurred in free-P_2O_5 specimen ($n = m = 1$) whereas by incorporating small amount of P_2O_5, the second crystallization peak evolves to a bulk crystallization.

Table 3
Activation energies (kJ.mol^{-1}), n and m parameters of each exothermic peak (Pk) for the studied specimens (n and m calculated from equation (1) and equation (2), respectively).

		Activation energy (kJ/mol)	n	m
MP0	**Pk1**	346.22	1.07	1.05
	Pk2	403.85	0.87	0.89
MP1	**Pk1**	361,83	1.12	0.95
	Pk2	485.82	1.93	1.86
MP2	**Pk1**	291.88	1.02	0.94
	Pk2	439.45	1.89	1.92
MP3	**Pk1**	177.16	1.29	0.82
	Pk2	231.63	1.82	1.73

3.1.4. *Spectroscopic characterization*

The microstructural changes occurring during the thermal conversion are studied by spectroscopic techniques. FTIR spectra recorded in the spectral region 1500–400 cm^{-1} are presented in Fig. 5 and the assignment of each band in the spectra to the corresponding bending or stretching vibrations are summarized in Table 4. In this range, the spectra of the base glasses exhibit three broad absorbance bands and a shoulder and their broadness are characteristic of a high percentage of amorphous glass. Mg^{2+} and K^+ ions act as network modifiers, inducing NBOs, and lying in interspaces of the glass network. Al^{3+}, as a network former, can substitute Si^{4+} to form [AlO_4] tetrahedron [39,40]. As the molar ratio of $Al_2O_3/(MgO + K_2O)$ is less than 0.5, [AlO_4] tetrahedron is easy to form in the investigated samples. The most intense band in the spectra present its maximum at 1020−1030 cm^{-1} and is attributed to the combination of the asymmetric stretching vibration of two types of bridging bonds Si–O(Si), Si–O(Al) and broken bridges Si–O$^-$ and Al–O$^-$ [41]. At about 1090 cm^{-1} the asymmetric stretching of Si–O–Si bond in [SiO_4] tetrahedron [42] or asymmetric stretching of P–O–P groups [43] is also detected and, the bands at 1180 cm^{-1} and 1270 cm^{-1} attributed to the stretching vibrations of Si═O [44] and the asymmetric stretching vibration of [BO_3] units [16] are common features of all the glasses. This main band in the spectra shifts from 1016 to 1029 cm^{-1} as the amount of P_2O_5 increases in the glasses. Additionally, the bands in the region of 800–650 cm^{-1} come from stretching vibration of Al–O bond in [AlO_4] tetrahedron and/or symmetrical stretching vibrations of Si–O–(Si,Al) and vibrations related to presence of silico-oxygen and alumino-silico-oxygen rings [16,45]. The shoulder near 560 cm^{-1} could be attributed to either stretching vibration of [MgO_4] [46] or to the bending vibration of the Al–O bond in [AlO_6] [42]. In Fig. 5 a, it is observed that by increasing the P_2O_5 amount, the relative intensity of the region 600−400 cm^{-1} assigned to bending vibration of O–Si–O linkages and Si–O–Si-bending vibration modes of [SiO_4] unit [16,47] decreases in intensity.

By increasing the temperature (Fig. 5 b), the band attributed to bending vibrations of O–Si–O and O–Al–O [44] and centred at 470 cm^{-1} increases in intensity and several additional bands near 688, 760 and 802 cm^{-1} and attributed to vibrations of 4 and/or 6-membered silico- and alumino-silico-oxygen rings [44], bending vibration of Al–O–Al in [AlO_4] tetrahedron [47] and symmetric stretching vibration of Si–O–Al bond [42] become more differentiated. At 850 °C (Fig. 5 c) the remanence of the three bands implies that the crystallization of the glass-ceramic has not yet come to the end, contrary to what occurs in the materials heat treated at 950 °C (Fig. 5 d), where multi-component bands appeared in the region 1400–800 cm^{-1} thus suggesting an increased mineralogical complexity. In these spectra, it can be found that some new absorption bands appear at about 890, 838, 612 and 515 cm^{-1} corresponding to forsterite [48] whereas he bands near 1176, 840 and 470 cm^{-1} can be interpreted as vibration modes in fluor-phlogopite [49]. With the increase of crystallization temperature, the contents of forsterite increase, while the contents of fluor-phlogopite decreases.

Fig. 6 shows the Raman spectra in the range of 300–1400 cm^{-1} of the base glasses and those thermally treated samples at 750, 850 and 950 °C for 1 h. A broad band in the range of 1200−800 cm^{-1} dominates the spectra of the as-prepared glasses (Fig. 6 a). By heating at 750 °C (Fig. 6 b) it is appreciated that the band becomes narrower suggesting an

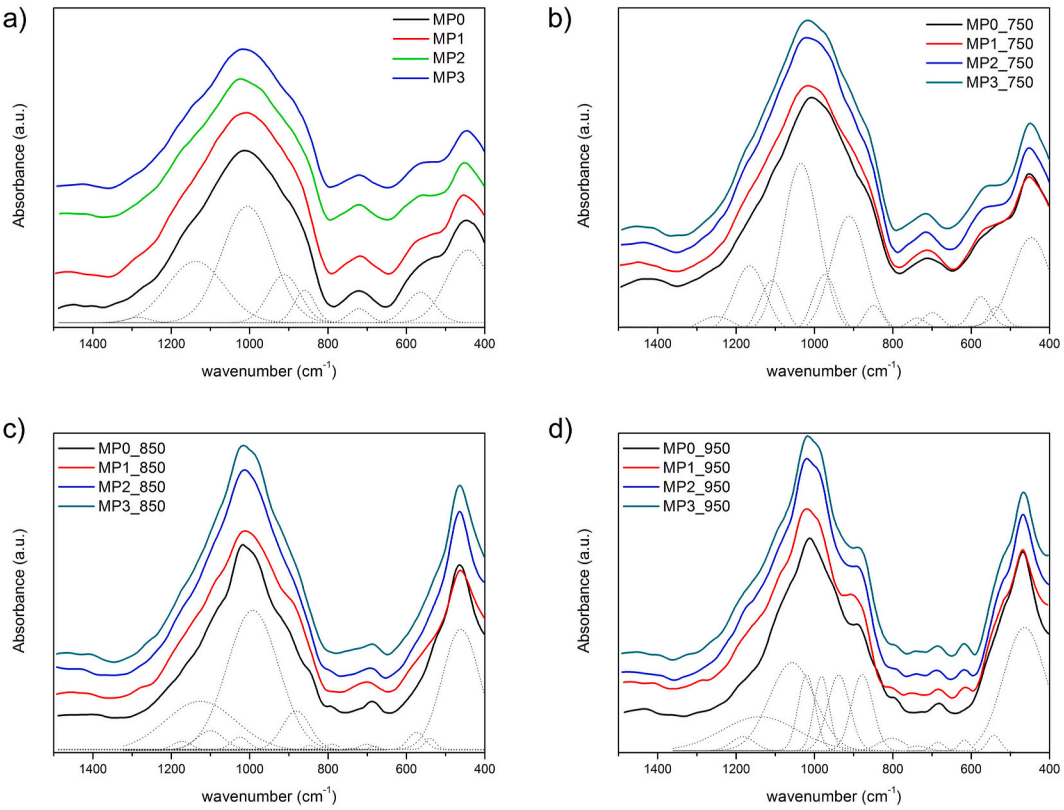

Fig. 5. FTIR spectra of the samples MP0, MP, MP2 and MP3 treated at a) as-prepared, b) 750, c) 850, and d) 950 °C. In dotted lines, there is shown an example of the deconvoluted spectra, by assuming Gaussian-shaped bands.

Table 4
Assignment of the main bands in the FTIR spectra.

Wavenumber transition (cm^{-1})	Assignment	Reference
1270	ν_{as} BO_3	[44]
1180	ν_{as} (SiO)	[43]
1176	ν_{as} (SiO) phlogopite	[49]
1090	ν_s (SiOSi) tetrahedron ν_{as} (POP)	[42]
1020–1030	ν_s (SiO–Si,Al)	[41,45]
890	ν_s (SiOSi) forsterite	[48]
840	SiO_4 phlogopite	[49]
838	SiO_4 b forsterite	[48]
760	AlO_4 tetrahedron	[44,45]
688	4,6 rings SiO–Si,Al	[44]
612	SiO_4 b forsterite	[48]
515	δ (OSiO) forsterite	[42,46]
470	δ (OSiO) phlogopite	[44,49]

incipient crystallization in the material but not yet consolidated. By further annealing at 850 °C (Fig. 6 c), the absorption band at 683 cm^{-1} attributable to fluor-phlogopite [49] is more evident in the case of MP0 material and decreases in intensity as the amount of P_2O_5 increases in the material. The bands at 276, 320, 683 and 1034 cm^{-1} are also attributed to the fluor-phlogopite crystals [49]. In the materials containing larger amounts of P_2O_5, two medium-intensity bands at 832 and 858 cm^{-1} are also visible, which are attributed to forsterite crystals that possess a characteristic set of two bands, near 858 cm^{-1} which correspond to Si–O asymmetric stretching band (Si–$O_{a\text{-}str}$) and ~832 cm^{-1} which correspond to Si–O symmetric stretching band (Si–$O_{s\text{-}str}$). Annealing at 950 °C (Fig. 6 d), results in an increase in the intensity of the bands corresponding to fluor-phlogopite for the low-containing P_2O_5 samples whereas the forsterite bands dominate the spectra of the materials containing higher amount of this nucleating agent.

3.2. Morphology in mica-containing glass-ceramics

FE-SEM photomicrographs of the etched surfaces of the base glasses are shown in Fig. 7. There, it can be observed the characteristic structure of a spinodal phase separation where two continuous phases take part of the microstructure, being one dissolved by HF whereas the remaining phase non affected by the etching process is the one observed under the microscope. This spinodal phase separations coarsened considerably by increasing P_2O_5 content to 2.0 and 3.0 mol%, As reported by Harper and McMillan [50] phase separation prior to crystallization in the Li_2O–SiO_2 system takes place when P_2O_5 was added at 1.0 and 2.0 mol%. Such phase separation causes the inner energy to decrease and enhances the degree of ordering inside the glass and therefore the thermodynamic stability of the system [51].

The microstructures of the different heat-treated glass-ceramics are presented in Fig. 7 e-h. The sample MP0 treated at 850 °C for 4 h (Fig. 7 e) possess a different crystalline morphology than MP1, MP2 or MP3, that present a *flower-like* crystals structure embedded in the glassy matrix. The average diameter of the *flower-like* crystals increased with increasing the P_2O_5 content, from 22 μm in MP1, ~26 μm in MP2 to 47 μm in MP3. In the case of MP0, it is observed a *dendritic-like* network having a *leaf-like* feature which is also comprised by aggregates of fine crystallites.

The EDX analysis of the GC allows distinguishing different elemental concentrations distributed along the surface. As shown in Fig. 8, several elemental determinations have been carried out in different points distributed all through the surface. In sample GC MP0, obviously, no P has been detected and the F atoms seem to be located preferably at the bright areas. In the remainder samples, it can be appreciated that the *flower-like* crystals are preferably enriched in F. At a position in close proximity to the *flower-like* crystal, the composition of the matrix is different and possesses a much smaller F concentration. According to these results, the positions enriched in F became deficient in P and vice-

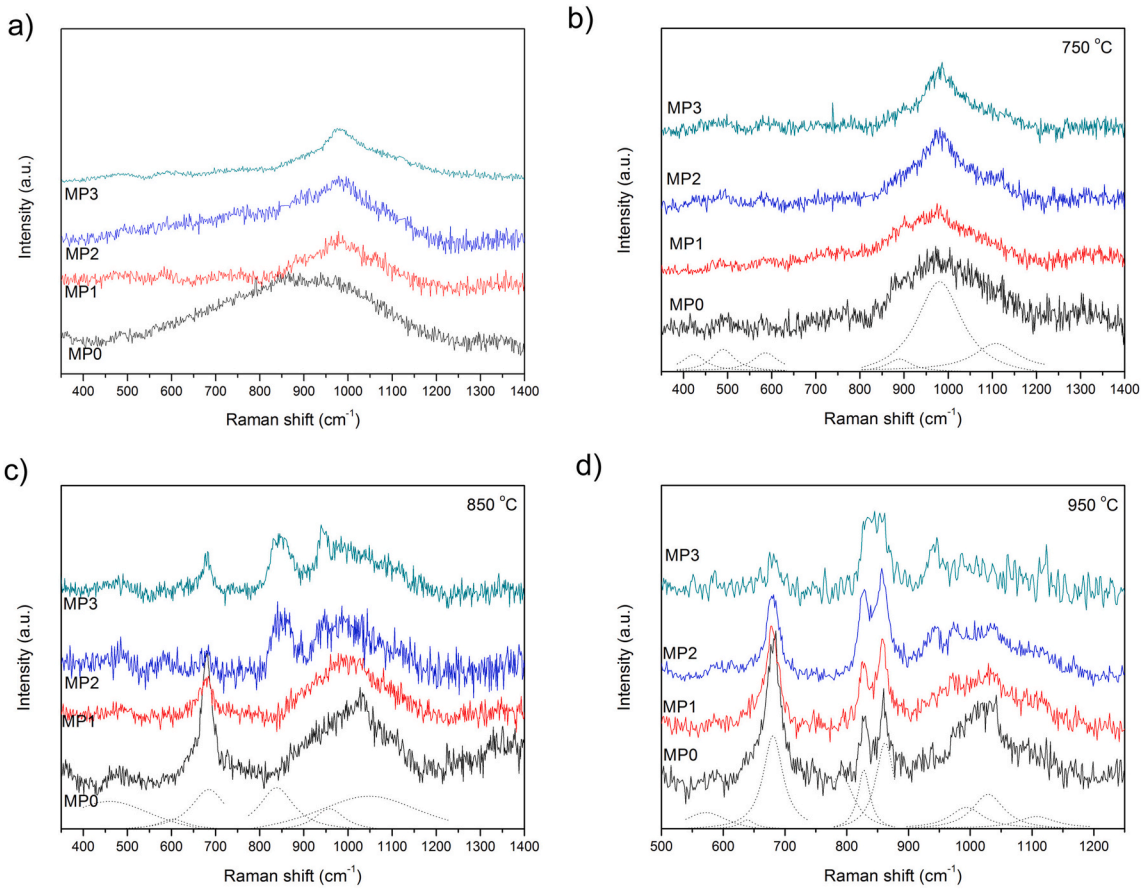

Fig. 6. Raman spectra of the samples MP0, MP, MP2 and MP3 treated at a) as-prepared, b) 750, c) 850, and d) 950 °C. In dotted lines (Fig. 6 b, c and d), there is shown an example of the deconvoluted spectra, by assuming Lorenztian-shaped bands.

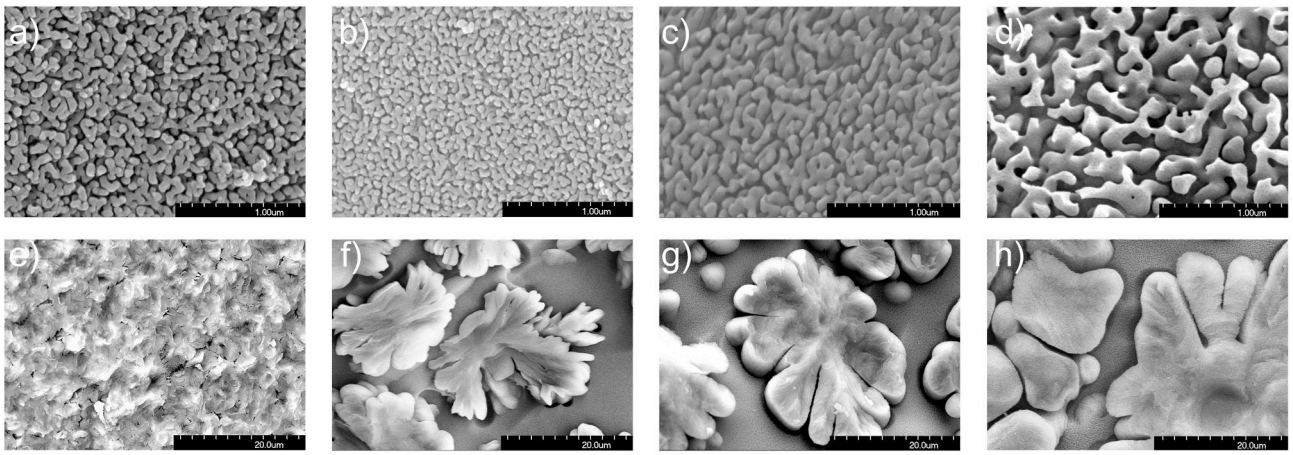

Fig. 7. FE-SEM images of the base glasses a)MP0, b) MP1, c) MP2 and d) MP3 and images of the glass ceramics obtained at 850 °C e) MP0, f) MP1, g) MP2, h) MP3.

versa. It is also evident in Fig. 7 and in Fig. 8 that the *flower-like* crystals have different sizes. Each *flower-like* crystal is composed of almost round areas (petals) extending to several microns connected and arranged in a circle around the centre. It is likely that petals are composed of aggregates spherical shaped nanocrystallites. The average size of nanocrystallites which was estimated using the Scherrer equation increased approximately from 18 (±0.5), 21 (±1) to 22 (±0.7) nm for the samples MP1, MP2 and MP3, respectively, with the increase of P_2O_5 content.

3.3. Mechanical properties

Nanoindentation test revealed a general decrease in the hardness of the GC with respect to the base glasses (Fig. 9). Berkovich hardness decreases progressively with the increase of P_2O_5 content in both the base glasses and the GC from 9.76 to 8.84 GPa and from 9.16 to 8.46 GPa, respectively and increases again to 9.70 GPa in the case of the base glasses and to 8.84 GPa in the GC at the maximum content of P_2O_5. This may be correlated with the crystalline composition of the CG. The reported Berkovich hardness for single crystals of phlogopite 2–2.5 GPa

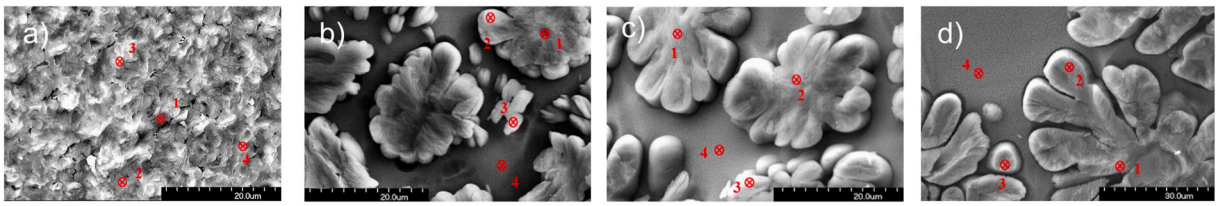

	MP0				MP1				MP2				MP3			
	1	2	3	4	1	2	3	4	1	2	3	4	1	2	3	4
Si	15,27	15,35	15,51	16,05	15,51	14,23	15,52	17,52	13,01	12,56	13,78	16,68	13,03	12,96	13,74	16,43
Mg	18,81	14,38	13,48	14,67	12,27	11,8	11,77	9,46	13,21	12,81	12,46	11,06	12,30	12,72	11,84	10,29
Al	3,74	5,62	5,28	5,74	5,65	5,38	6,25	6,50	6,13	5,85	6,17	7,32	5,92	5,55	6,34	6,88
F	4,73	8,67	9,03	6,28	6,15	10,35	6,74	3,29	11,17	13,63	8,94	0,65	8,82	11,13	8,19	1,65
K	1,67	1,65	2,85	1,25	4,61	3,83	2,84	3,02	2,13	2,23	2,70	1,44	2,80	2,27	2,88	1,63
P	-	-	-	-	0,46	0,32	0,45	1,08	0,59	0,76	1,03	1,92	1,03	0,68	0,92	2,52

Fig. 8. EDX analysis of the GC a) MP0 b) MP1 c) MP2 and d) MP3.

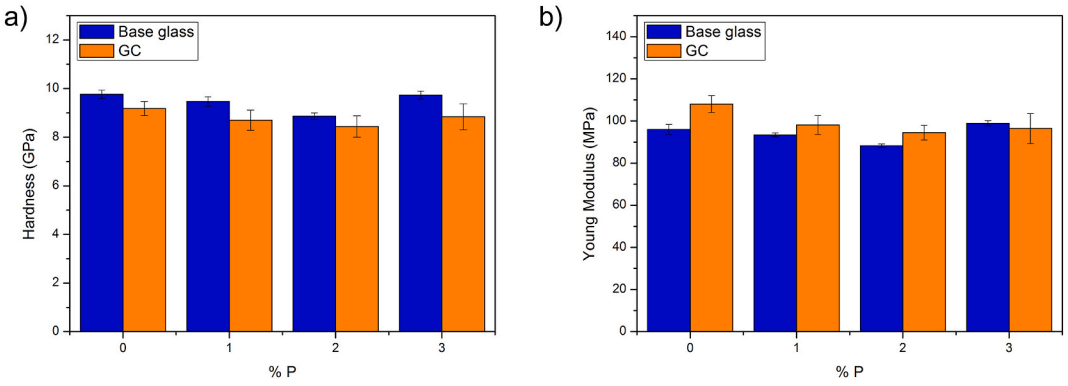

Fig. 9. Mechanical properties of the materials as calculated by nanoindentation tests.

whereas in sintered forsterite ceramics, the maximum hardness is found to be about 7.7 GPa [52,53] On contrary, the Young Modulus of the GC is slightly higher in the GC than the base glasses, and although in the base glasses it experiments the same behavior as the hardness values, the Young Modulus decreases continuously with the amount of P_2O_5. In the base glasses, the Young Modulus varies from 88 to 99 MPa whereas in the case of the GC, these values are comprised between 94 and 108 MPa. These values are in perfect agreement with some others reported in the literature [54].

3.3.1. *Optical characteristics of the GC*

Several visual changes in the appearance of the base glasses and GC upon P_2O_5 addition were noticed at a first sight. The MP0 base glass was transparent and homogeneous with a yellowish appearance, similar to MP1. Increasing the P_2O_5 content leads to semi-translucent opaline, and white opaline glasses in MP2 and MP3 glasses, respectively. When the P_2O_5 content is more than 1.0 mol%, the change of transparency may be caused by excessive phase separation effect of P_2O_5. The transparency then decreases by increasing P_2O_5 content up to 1.0 mol% accompanied by a colour change from yellowish transparent to white opaline. As shown in Table 5, the refraction index of the base glasses is about 1.4 and decreases progressively with the P_2O_5 content. In the GC, after a first increase of the refractive index in the material containing 1% P_2O_5, the refraction index decreases again due to the change in the composition of the crystalline phases.

Table 5
Refraction index of the base glasses and the GC.

		MP0	MP1	MP2	MP3
n_D	Base glass	1.5420	1.5417	1.5396	1.5365
	Heat-treated at 750 °C for 3 h	1.5422	1.5441	1.5408	1.5391

The transmittance spectra of the base glass and GC heat treated at 750 °C are shown in Fig. 10 a and b, respectively. In the spectra, there is no sharp absorption edge in the spectra, which characterizes the glassy nature of samples [55]. It is also observed that the transmittance of MP0 reaches a transmittance value of approximately 88% in the visible range. The increase in the transmittance in the λ~320–400 range is slightly sharper after the incorporation of (1.0 mol%) P_2O_5 whereas by further increasing the P_2O_5 content, the transmittance experiments a smooth increases with the wavenumber reaching transmittance values of about 60% (MP2) and 40% (MP3) at the end of the visible range.

From the transmission spectra, the colour parameters of both the parent glasses and the GC have been calculated using the International Commission on Illumination (CIE) L*, a*, b*. The corresponding chromatic coordinate values are represented in Fig. 10 c. The MP0 and MP1 samples are characterized by lower values of a^* and b^* indicating a tendency to achromatism whereas the increase of P_2O_5 content leads to a slight shift to reddish colour.

The optical band gap energy (E_v) of each sample was calculated from Tauc's plot using the data obtained from UV–Visible spectroscopy (Fig. 10 a and b). The relation between absorption coefficient (α) and incident photon energy ($h\nu$) was used as proposed by Mott and Davis [56]:

$$\alpha = K\frac{(h\nu - E_v)^n}{h\nu} \quad \text{Equation 3}$$

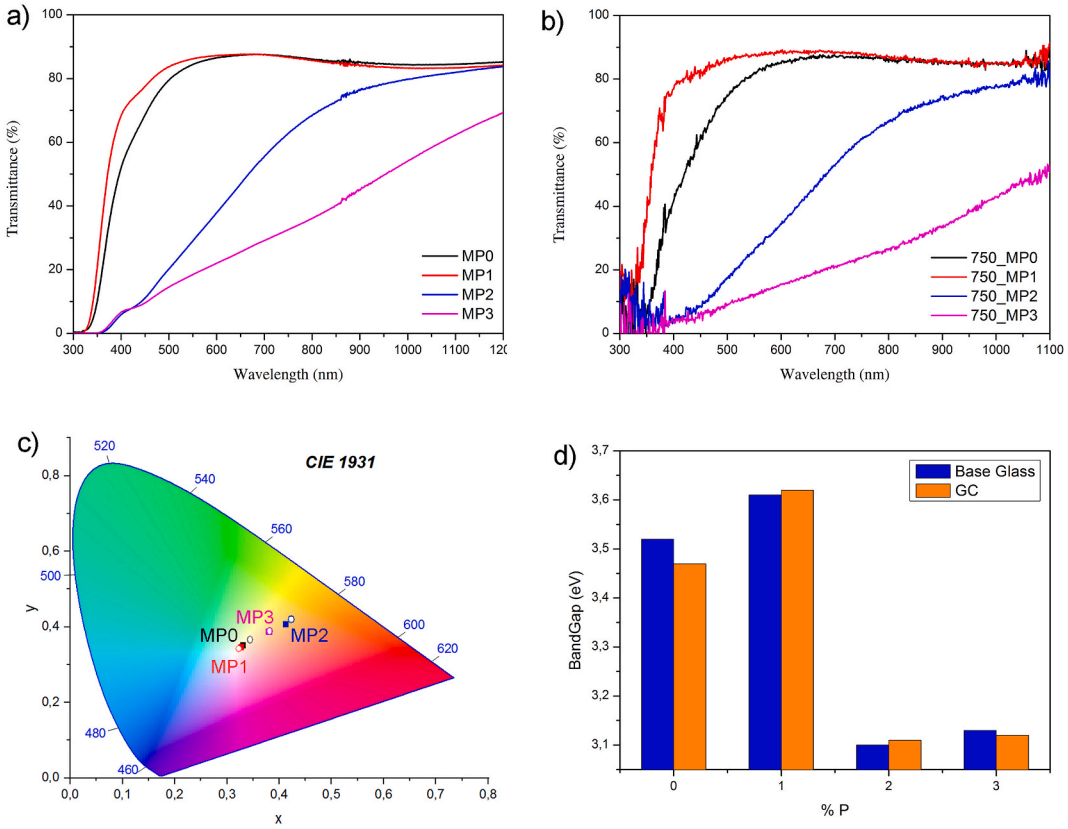

Fig. 10. a) Transmittance spectra of the base glass, b) Transmittance spectra of the corresponding GC c) chromatic coordinate values of the base glasses (as solid spots) and the corresponding glass ceramics (as open spots).

where K is a constant, and n is the index, whose value depends on the type of the transition taking place that as 2, 3, 1/2 and 3/2 representing indirect allowed, indirect forbidden, direct allowed and direct forbidden transitions, respectively. In this work, direct allowed transitions (n = 1/2) is valid based on Tauc relations [57]. From the plot of $(\alpha h\nu)^2$ against the photon energy ($h\nu$) and the intercept with the X-axis of the linear portions of the obtained curves, the energy band gap of optical transitions have been calculated and presented in Fig. 10 d. There, it can be observed that either in the base glass and the GC, the energy band gap reaches values above 3.6 eV for those containing 1% P_2O_5 and then, after a small increase in the amount of this nucleating agent, the band gap experiments a strong decrease reaching values of about 3.10 and 3.13 eV in the MP2 and MP3 samples, respectively. These observations must be attributed to the network structural differences brought by the additional presence of phosphorus ions.

4. Discussion

The addition of fluorine and phosphorus compounds to glass materials is a strategy commonly used for obtaining opaline and frosted glasses [58]. In addition, the light transmission of the material depended on the phosphorus oxide content [59]. In this work, mica-containing glass ceramics have been obtained through the addition of MgF_2 and P_2O_5 nucleating agent. As confirmed by X-ray results (Fig. 1), the base glasses remain amorphous and the phase separation is effectuated by liquation. In the prepared glasses, fluor-phlogopite appeared at temperatures as low as 800 °C and forsterite crystalline phase is formed at the temperatures beyond 900 °C. In the material with the highest P_2O_5 content, the precipitation of fluor-phlogopite and forsterite appeared at 750 °C and 800 °C respectively, a fact that is attributed to the decrease in the viscosity of the glasses. The nucleating agent P_2O_5 can thus promote the presence of fluor-phlogopite and forsterite at lower temperatures compared to the remainder sample reducing the activation energy of both crystal phases in this system. More intense reflections of forsterite appeared at 950 °C, being indeed forsterite the master phase in the GC samples at higher temperatures. This observation contradicts to the reported by Cho et al. [60] who found that some deliberate nucleating agents including P_2O_5 were inactive and did not participate in the nucleation process. Forsterite crystals containing Mg^{2+} ions are also precipitated when crystallization temperature increased. It is possibly due to the increasing of Mg^{2+} ions mobility from the decomposition of fluor-phlogopite, resulting in the formation of forsterite, as observed by Faeghi-Nia et al. [61]. Mg^{2+} can induce the non-uniform arrangement of anionic charge [39]. Mg^{2+} and K^+ ions help to the balance of $[AlO_4]^-$ tetrahedron, contributing to the formation of $[AlO_4]_2Mg$ and $[AlO_4]K$ complexes in glass networks [16].

It is reported that glasses with a P_2O_5 content of 0.0 and 0.5 mol% present a surface crystallization mechanism [62] whereas in the LAS system, however, trace amounts of P_2O_5 transforms the system to a bulk crystallization [63]. The data collected in Table 3 regarding the n and m values indicate that the incorporation of P_2O_5 leads to a homogeneous crystallization mechanism for both exothermic peaks and mainly with one- and two-dimensional growth of crystals. In addition, it has been demonstrated that glasses that display only surface crystallization have a reduced glass transition temperatures, $T_{rg}(= T_g/T_m$, where T_m is the melting temperature), higher than approximately 0.58–0.60, whereas glasses with $T_{rg} < 0.58$ exhibit volume crystallization [64]. The T_{rg} obtained for the base glasses summarized in Table 2 indicates that the P_2O_5 content has a considerable effect on the value of T_{rg} due to the changes in the viscosity of the glasses. As reported by Glatz et al. depending on the concentration of P_2O_5 with respect of other components in the glasses and GC, T_g will appear at higher or lower temperature [65]. In LMAS GC containing Li_2O–MgO–Al_2O_3 plus F, CaO, ZrO_2 and TiO_2, there occurs a bulk-type crystallization and the T_g increases as

the P_2O_5 content does [29], however, in LAS GC, Tg decreases as P_2O_5 content is raised [66]. In the prepared GC, an increase in P_2O_5 content leads to a change in the crystallization process of these glasses, from a mechanism of surface crystallization that is predominant in MP0 (the value of T_{rg} is near to 0.58) to a prevailing volume crystallization in MP1, MP2 and MP3. The incorporation of P_2O_5 to the base glasses restrains the surface crystallization and promotes bulk crystallization.

In the present work, there is a possibility of vaporization of fluorine during melting and crystallization of the glasses. Treatment at higher temperature showed an increase in the crystallinity but with relative decrease in fluorinated phase's contents. The fluorine loss at glass composition can be resulted in magnesium and silicon rich phase corresponds to forsterite formation. In Table 1, there is reported the amount of fluorine remaining in the glasses after the thermal treatment. It is observed that the amount of fluorine slightly decrease from 3.90 to 3.30% independently of the P_2O_5 amount. According to Wood et al. [67] volatile silicon tetrafluoride from the surface glass causes the re-dissolution of the fluorphlogopite phase and the crystallization of fluorine-free phases rather than the fluorphlogopite. In addition, Kodaira et al. [68] reported that fluorine deficiency causes fluormica compounds to decompose to forsterite. On its side, Mirsaneh et al. [26] have reported that less mica formed when more P_2O_5 was added to mica glass-ceramic. In consequence, mica crystallization is affected by the sole addition of P_2O_5 and the fact that the amount of F remains more or less constant in the materials suggest that the addition and increasing amounts of P_2O_5 will induce forsterite surface crystallization as predominant phase particularly at high temperatures. The promotion of the surface crystallization, as occurs in the P_2O_5-free GC will therefore decrease the loss of the SiF_4 thus increasing the stability of the material at high temperature.

According to the FTIR and Raman results (Figs. 5 and 6) the band appearing at 880−887 cm^{-1} is associated with asymmetric stretching vibrations of Si–O^- and Al–O^- [44], and the band near 990 cm^{-1} corresponds to the stretching vibrations of Si–O-(Si) [44]. The excellent compatibility between the complexes and [SiO_4] tetrahedron facilitates the formation of mica units [$AlSiO_3$]. The experimentally calculated activation energies (for T_{c1} and T_{c2}) of the base glasses (see Table 3) have been matched well with the single bond strengths of Al–O (222 kJ mol^{-1}), Mg–O (154 kJ mol^{-1}), and Si–O (428 kJ mol^{-1}) present in crystal phases formed in the resultant glass-ceramics.

Early study indicated that liquid–liquid phase separation occurred with Mg^{2+} and K^+ containing glass-ceramics [15]. Mg^{2+} has higher cationic field strength compared with K^+ and then the addition of MgF_2 tends to phase separation, which improved the nucleation and crystallization of glass. Each phase has a different chemical composition and is enriched of one or more chemical components compared to the surrounding phase. This inference is confirmed by the EDS analysis of the base glasses (Fig. 8). The addition of small amount of P_2O_5 (1.0 mol%) to these glass-ceramics changed the microstructure to a characteristic *flower-like* pattern. The difference in both morphologies (presented in Fig. 7) lies in the respective crystallization mechanisms. The crystallization mechanism related to crystallization process is found to be one-dimensional growth with a fixed number of nuclei for MP0 and two-dimensional growth with a constant nucleation rate for MP1, MP2 and MP3. In addition, P^{5+} can promote the glass to separate into two different composition areas. According to the EDS observation (Fig. 8), the concentration of P in the *flower-like* area is considerably lower than in the residual glass. Glendenning and Lee [69] found that the high charge density of P^{5+} indicates that it may be difficult to incorporate into the crystal phase. Although P_2O_5 was added intentionally, it was not found in the crystalline phases at 850 °C by the XRD results (Fig. 1), which revealed that P^{5+} exist in the residual glass and P_2O_5 did not participate in nucleation process.

The base glasses show low refractive index (in the range 1.5368–1.5431). The refractive index decreases gradually with the increase of P_2O_5 content. When heated for 3 h at 750 °C, the refractive index increases after the formation of crystallites. It can be found that, the refractive index of the fluor-phlogopite crystals (1.53–1.573) and the glass phase is almost similar. This similarity favours a low light scattering. Thus, it is valid that the refractive index slightly increases for the formation of crystals. What is more, the continuous variation in glass and crystal compositions during crystallization and probably the effect of the high charge density of P^{5+} cause a small change of the refractive index with the increase of P_2O_5 content.

The E_v depends on the surrounding metal ions and the concentration of BO and NBO atoms. The increase of E_v in MP1 is probably related to the formation of NBOs which are substituting BO atoms, then the system has made it easier for the electrons to move through the materials [70]. A similar increase in the content of NBO has been reported for glassy silica by introduction of small quantities of P_2O_5 [71]. Hence, reduction of E_v by increasing P_2O_5 content (>1.0 mol%) of samples was attributed to the enhancement of ionic bonds in the matrix and formation of more ordered structure due to the creation of BOs [70]. The MP2 and MP3 base glasses have lost their transparency due to the formation of a coarser spinodal phase separation caused by P_2O_5, and the consequent increase in the intensity of scattering light and the decrease in the transmission of visible light. The transmittance in the ultraviolet range falls at the low wavelength range, and the corresponding absorption phenomena are associated with the number of BOs, absorption limit shifts to the long wavelength in the case of less BOs [67]. Moreover, the optical cut-off of MP0 and MP1 is 315 nm, and shifts to ~360 nm in MP2 and MP3. As mentioned in Ref. [72], the change of transparency of LAS glass-ceramic system (LAS: $Li_2O-A1_2O_3–SiO_2$) is caused by excessive phase separation due to the excess P_2O_5 (more than 4 wt%), which confirmed our results. in contrast, when the P_2O_5 content is 1.0 mol%, the transmission increase with respect to MP0, showing that the limited phase separation effect caused by P_2O_5 has a positive impact on the transparency. It is well known that the optimum nucleation temperature lies between T_g and T_d, therefore, one stage heat-treatment at 750 °C was selected, in order to obtain glass-ceramics containing microcrystals, consequently keep transparency of the glass.

After heat-treatment process, the optical energy gap slightly decreases for the MP0 however it is nearly constant in MP1, MP2 and MP3. Therefore, the fine particles corresponded to the fluor-phlogopite crystallites, and the glass-ceramic displayed a good transparency. Assuming that during the primary stage of crystallization event, droplets of fluorphlogopite first nucleate. When heated for 3 h at 750 °C, the samples maintained the same characteristics as the base glasses; there is no visible change. It is clear from Fig. 10 that the transmittance is reduced by the heat-treatment. That is, nano-crystallites precipitated in the glass-ceramic samples can scatter the visible ray. If we consider that no heat-treatment optimization has been carried out, adding (1.0 mol%) of P_2O_5 allowed the production of highly homogeneous initial glass and the increase in the transmittance of MP1 glass-ceramic with respect to the MP0 sample is of great advantage for certain applications. Yekta et al. [25] have reported that the mica crystals morphology can changed from platelet to spherical shapes by addition of PbO and P_2O_5 to the base glasses. Hence, it undergoes a dendritic growth into the MgO-rich matrix in the glass of this system. Then, it ends by conglomeration of adjacent crystalline areas (petals), and results in producing two-dimensional *flower-like* crystals over the phase-separated areas. Further identification by XRD and FESEM–EDS and some more detailed studies on the possible mechanism for the development of this microstructure are needed and they will surely lead to a better understanding the generation of this unusual crystal morphology in this system.

5. Conclusion

Form these results, it can be concluded that P_2O_5 additive performs better than free-P_2O_5 for improving crystallization ability (lowering the activation energy of crystallization), which also could promotes crystallization at lower temperatures because of the decrease in the viscosity

of the glasses. Consequently, the base glasses have the spinodal phase separation, which coarsened considerably by increasing P_2O_5 content. The predominant crystalline phase is fluor-phlogopite [$KMg_3(Si_3AlO_{10})F_2$] in the absence of P_2O_5 and gradually transforms to forsterite by increasing P_2O_5 concentration. The amount of P_2O_5 added can affect the crystal size of glass-ceramics. The heat-treatment schedule has the obvious effect on the properties of glass-ceramics. The content of precipitated phase becomes higher with rising of crystallization temperature.

The crystallization mechanism based on the calculation of the Avrami exponent is found to be one-dimensional growth with a fixed number of nuclei for MP0 and two-dimensional growth with a constant nucleation rate for glass-ceramics with P_2O_5. In P_2O_5-free glass-ceramic a the dendritic growth of the aggregated particles is observed, while, MP1, MP2 and MP3 glass-ceramic specimens show predominant *flower-like* fluor-phlogopite mica crystal. The crystallization process changes from a mechanism of surface crystallization that is predominant in the MP0 to a prevailing volume crystallization in glass-ceramics with P_2O_5. P^{5+} decreases the precipitation temperature of fluor-phlogopite and forsterite in K_2O–MgO–Al_2O_3–B_2O_3–SiO_2–MgF_2 system from 800 to 750 °C and from 900 to 800 °C, respectively. With the optimum amount of nucleating agent, which is found to be 1.0 mol% P_2O_5, colourless glass-ceramics with about 80% transmittance at visible light spectra can obtained by the one stage heat-treatment at 750 °C for 3 h.

Declaration of competing interest

The authors declare that they have no known competing financial interests or personal relationships that could have appeared to influence the work reported in this paper.

Acknowledgements

This work has been developed with the financial support of the project “Fertilizantes Sostenibles Frente al Cambio Global” INCGL20033 framed within the program Plan de Colaboración Internacional from the Spanish National Research Council.

References

[1] W. Höland, E. Apel, C. van’t Hoen, V. Rheinberger, Studies of crystal phase formations in high-strength lithium disilicate glass–ceramics, J. Non-Cryst. Solids 352 (2006) 4041–4050.
[2] H. Bach, D. Krause, Analysis of the Composition and Structure of Glass and Glass Ceramics, Springer Science & Business Media, 2013.
[3] D.P. Mukherjee, S.K. Das, Influence of TiO2 content on the crystallization and microstructure of machinable glass-ceramics, J. Asian Ceramic Soci. 4 (2016) 55–60.
[4] S. Roy, B. Basu, Microstructure development in machinable mica based dental glass ceramics, Trends Biomater. Artif. Organs 20 (2006) 90–100.
[5] D.G. Grossman, Machinable glass-ceramics based on tetrasilicic mica, J. Am. Ceram. Soc. 55 (1972) 446–449.
[6] R. McNally, G. Beall, Crystallization of fusion cast ceramics and glass-ceramics, J. Mater. Sci. 14 (1979) 2596–2604.
[7] M. Garai, N. Sasmal, A.R. Molla, S. Singh, A. Tarafder, B. Karmakar, Effects of nucleating agents on crystallization and microstructure of fluorophlogopite mica-containing glass–ceramics, J. Mater. Sci. 49 (2014) 1612–1623.
[8] K. Cheng, J. Wan, K. Liang, Enhanced mechanical properties of oriented mica glass-ceramics, Mater. Lett. 39 (1999) 350–353.
[9] S. Taruta, T. Ichinose, T. Yamaguchi, K. Kitajima, Preparation of transparent lithium-mica glass-ceramics, J. Non-Cryst. Solids 352 (2006) 5556–5563.
[10] P. Alizadeh, V. Khani, Crystallization kinetics and characterization of nanostructure mica glass-ceramics with optical transparency, J. Nanostruc. 4 (2014) 45–53.
[11] A.F. Nia, Thermal properties and crystallization of lithium–mica glass and glass-ceramics, Thermochim. Acta 564 (2013) 1–6.
[12] S. Taruta, K. Mukoyama, S.S. Suzuki, K. Kitajima, N. Takusagawa, Crystallization process and some properties of calcium mica–apatite glass-ceramics, J. Non-Cryst. Solids 296 (2001) 201–211.
[13] W. Höland, W. Vogel, W. Mortier, P.-H. Duvigneaud, G. Naessens, E. Plumat, A new type of phlogopite crystal in machineable glass ceramics, Glass Technol. 24 (1983) 318–322.
[14] G.H. Beall, L.R. Pinckney, Nanophase glass-ceramics, J. Am. Ceram. Soc. 82 (1999) 5–16.
[15] M. Ghasemzadeh, A. Nemati, S. Baghshahi, Effects of nucleation agents on the preparation of transparent glass–ceramics, J. Eur. Ceram. Soc. 32 (2012) 2989–2994.
[16] L. Yu, H. Xiao, Y. Cheng, Influence of magnesia on the structure and properties of MgO-Al2O3-SiO2-F− glass-ceramics, Ceram. Int. 34 (2008) 63–68.
[17] H.M. Fathi, A. Johnson, The effect of TiO2 concentration on properties of apatite-mullite glass-ceramics for dental use, Dent. Mater. 32 (2016) 311–322.
[18] A.V. DeCeanne, L.R. Rodrigues, C.J. Wilkinson, J.C. Mauro, E.D. Zanotto, Examining the role of nucleating agents within glass-ceramic systems, J. Non-Cryst. Solids 591 (2022), 121714.
[19] D.P. Mukherjee, A.R. Molla, S.K. Das, The influence of MgF2 content on the characteristic improvement of machinable glass ceramics, J. Non-Cryst. Solids 433 (2016) 51–59.
[20] L. Radonjić, L. Nikolić, The effect of fluorine source and concentration on the crystallization of machinable glass-ceramics, J. Eur. Ceram. Soc. 7 (1991) 11–16.
[21] S. Taruta, M. Suzuki, T. Yamakami, T. Yamaguchi, K. Kitajima, Preparation and ionic conductivity of transparent glass− ceramics containing a large quantity of lithium− mica, J. Non-Cryst. Solids 354 (2008) 848–855.
[22] K. Cheng, J. Wan, K. Liang, Crystallization of R2O–MgO–Al2O3–B2O3–SiO2–F (R= K+, Na+) glasses with different fluorine source, Mater. Lett. 47 (2001) 1–6.
[23] P. James, Glass ceramics: new compositions and uses, J. Non-Cryst. Solids 181 (1995) 1–15.
[24] A. Ananthanarayanan, A. Dixit, R. Lenka, R. Purohit, V. Shrikhande, G. Kothiyal, Some studies on the phase formation and kinetics in TiO 2 containing lithium aluminum silicate glasses nucleated by P 2 O 5, J. Therm. Anal. Calorim. 106 (2011) 839–844.
[25] B.E. Yekta, S.H. Nia, P. Alizadeh, The effect of B2O3, PbO and P2O5 on the sintering and machinability of fluormica glass–ceramics, J. Eur. Ceram. Soc. 25 (2005) 899–902.
[26] M. Mirsaneh, I.M. Reaney, P.V. Hatton, S. Bhakta, P.F. James, Effect of P2O5 on the early stage crystallization of K-fluorrichterite glass–ceramics, J. Non-Cryst. Solids 354 (2008) 3362–3368.
[27] P.K. Jha, O. Pandey, K. Singh, Structural and thermal properties of Na2S–P2S5 glass and glass ceramics, J. Non-Cryst. Solids 379 (2013) 89–94.
[28] O.V. Mazurin, Problems of compatibility of the values of glass transition temperatures published in the world literature, Glass Phys. Chem. 33 (2007) 22–36.
[29] K. Ariane, A. Tamayo, A. Chorfa, F. Rubio, J. Rubio, Effect of P2O5 and Al2O3 on Crystallization, Structure, Microstructure and Properties of Li2O–MgO–Al2O3–SiO2–TiO2–ZrO2 Glass Ceramics, Boletín de la Sociedad Española de Cerámica y Vidrio, 2020.
[30] L. Sun, J. Fang, S. Guo, T. Shan, Y. Wen, C. Liu, J. Zhang, Effect of MgO/Al2O3 ratio on the crystallization behaviour of Li2O–MgO–Al2O3–SiO2 glass-ceramic and its wettability on Si3N4 ceramic, Ceram. Int. 48 (2022) 20053–20061.
[31] M. Pascual, L. Pascual, Determination of the viscosity–temperature curve for glasses on the basis of fixed viscosity points determined by hot stage microscopy, Phys. Chem. Glasses 42 (2001) 61–66.
[32] A. Inoue, T. Zhang, T. Masumoto, Reductilization of embrittled La Al Ni amorphous alloys by viscous flow deformation in a supercooled liquid region, J. Non-Cryst. Solids 156 (1993) 598–602.
[33] M. Saad, M. Poulain, Glass Forming Ability Criterion, Materials Science Forum, Trans Tech Publ, 1987, pp. 11–18.
[34] H.E. Kissinger, Reaction kinetics in differential thermal analysis, Anal. Chem. 29 (1957) 1702–1706.
[35] K. Matusita, S. Sakka, Kinetic study of crystallization of glass by differential thermal analysis—criterion on application of Kissinger plot, J. Non-Cryst. Solids 38 (1980) 741–746.
[36] J. Augis, J. Bennett, Calculation of the Avrami parameters for heterogeneous solid state reactions using a modification of the Kissinger method, J. Therm. Anal. Calorim. 13 (1978) 283–292.
[37] T.S. Rao, T.L.S. Rao, A. Shaker, K. Venkatraman, Crystallization Kinetics of Amorphous Fe77B16Si5Cr2 Metallic Glass, Tc, 1 T2.
[38] A.R. Molla, B. Basu, Microstructure, mechanical, and in vitro properties of mica glass-ceramics with varying fluorine content, J. Mater. Sci. Mater. Med. 20 (2009) 869–882.
[39] C.I. Merzbacher, W.B. White, The structure of alkaline earth aluminosilicate glasses as determined by vibrational spectroscopy, J. Non-Cryst. Solids 130 (1991) 18–34.
[40] C. Huang, E. Behrman, Structure and properties of calcium aluminosilicate glasses, J. Non-Cryst. Solids 128 (1991) 310–321.
[41] M. Leśniak, J. Partyka, M. Sitarz, Impact of ZnO on the structure of aluminosilicate glazes, J. Mol. Struct. 1126 (2016) 251–258.
[42] H. Gui, C. Li, C. Lin, Q. Zhang, Z. Luo, L. Han, J. Liu, T. Liu, A. Lu, Glass forming, crystallization, and physical properties of MgO-Al2O3-SiO2-B2O3 glass-ceramics modified by ZnO replacing MgO, J. Eur. Ceram. Soc. 39 (2019) 1397–1410.
[43] L. Han, J. Song, C. Lin, J. Liu, T. Liu, Q. Zhang, Z. Luo, A. Lu, Crystallization, structure and properties of MgO-Al2O3-SiO2 highly crystalline transparent glass-ceramics nucleated by multiple nucleating agents, J. Eur. Ceram. Soc. 38 (2018) 4533–4542.
[44] J. Partyka, M. Leśniak, Raman and infrared spectroscopy study on structure and microstructure of glass–ceramic materials from SiO2–Al2O3–Na2O–K2O–CaO system modified by variable molar ratio of SiO2/Al2O3, Spectrochim. Acta Mol. Biomol. Spectrosc. 152 (2016) 82–91.
[45] J. Partyka, M. Leśniak, Preparation of glass–ceramic glazes in the SiO2–Al2O3–CaO–MgO–K2O–Na2O–ZnO system by variable content of ZnO, Ceram. Int. 42 (2016) 8513–8524.

[46] D. Pal, A. Chakraborty, S. Sen, S. Sen, The synthesis, characterization and sintering of sol-gel derived cordierite ceramics for electronic applications, J. Mater. Sci. 31 (1996) 3995–4005.
[47] L. Han, J. Song, Q. Zhang, Z. Luo, A. Lu, Crystallization, structure and characterization of MgO-Al2O3-SiO2-P2O5 transparent glass-ceramics with high crystallinity, J. Non-Cryst. Solids 481 (2018) 123–131.
[48] M. Leśniak, J. Partyka, K. Pasiut, M. Sitarz, Microstructure study of opaque glazes from SiO2–Al2O3–MgO–K2O–Na2O system by variable molar ratio of SiO2/Al2O3 by FTIR and Raman spectroscopy, J. Mol. Struct. 1126 (2016) 240–250.
[49] D.A. McKeown, I.S. Muller, A.C. Buechele, I.L. Pegg, C.A. Kendziora, Structural characterization of-high-zirconia borosilicate glasses using Raman spectroscopy, J. Non-Cryst. Solids 262 (2000) 126–134.
[50] H. Harper, P. James, P. McMillan, Crystal nucleation in lithium silicate glasses, Discuss. Faraday Soc. 50 (1970) 206–213.
[51] D. Hülsenberg, A. Harnisch, A. Bismarck, Microstructuring Glasses Using Lasers, Springer, 2008.
[52] K.S. Lee, K.C. Chin, S. Ramesh, J. Purbolaksonoa, M. Hassan, M. Hamdi, W. Teng, Characterization of forsterite ceramics, J. Ceram. Process. Res. 14 (2013) 131–133.
[53] M. Ghaffari, P. Alizadeh, M. Rahimipour, Sintering behavior and mechanical properties of mica-diopside glass–ceramic composites reinforced by nano and micro-sized zirconia particles, J. Non-Cryst. Solids 358 (2012) 3304–3311.
[54] S. Habelitz, G. Carl, C. Rüssel, S. Thiel, U. Gerth, J.-D. Schnapp, A. Jordanov, H. Knake, Mechanical properties of oriented mica glass ceramic, J. Non-Cryst. Solids 220 (1997) 291–298.
[55] A. Faeghinia, UV-vis absorption and luminescence spectrum of LAS: Tb3+/Gd3 as a laser material, Int. J. Eng. 27 (2014) 609–614.
[56] N. Mott, States in the gap in non-crystalline semiconductors, J. Phys. C Solid State Phys. 13 (1980) 5433.
[57] J. Tauc, Optical Properties of Amorphous Semiconductors, Amorphous and Liquid Semiconductors, Springer, 1974, pp. 159–220.
[58] E. Yatsenko, Mutual Influence of the Components of White Single-Layer Glass Enamels on the Opacification Mechanism, Glass & Ceramics, 2009, p. 66.
[59] E. Tsareva, M. Pirogova, Y.A. Spiridonov, Opacified and opaline enamels on precious metals, Glass Ceram. 68 (2012) 376–377.
[60] Y.S. Cho, W.A. Schulze, V.R. Amarakoon, Crystallization kinetics and properties of nonstoichiometric cordierite-based thick-film dielectrics, J. Am. Ceram. Soc. 82 (1999) 3186–3192.
[61] A. Faeghi-Nia, V. Marghussian, E. Taheri-Nassaj, Effect of B2O3 on crystallization behavior and microstructure of MgO–SiO2–Al2O3–K2O–F glass–ceramics, Ceram. Int. 33 (2007) 773–778.
[62] S.C. von Clausbruch, M. Schweiger, W. Höland, V. Rheinberger, The effect of P2O5 on the crystallization and microstructure of glass-ceramics in the SiO2–Li2O–K2O–ZnO–P2O5 system, J. Non-Cryst. Solids 263 (2000) 388–394.
[63] D. Holland, Y. Iqbal, P. James, B. Lee, Early stages of crystallisation of lithium disilicate glasses containing P2O5–An NMR study, J. Non-Cryst. Solids 232 (1998) 140–146.
[64] E.D. Zanotto, Bright future for glass-ceramics, Am. Ceram. Soc. Bull. 89 (2010) 19–27.
[65] P. Glatz, M. Comte, L. Cormier, L. Montagne, B. Doumert, G.G. Moore, Different roles of phosphorus in the nucleation of lithium aluminosilicate glasses, J. Non-Cryst. Solids 493 (2018) 48–56.
[66] X. Guo, H. Yang, C. Han, F. Song, Crystallization and microstructure of Li2O–Al2O3–SiO2 glass containing complex nucleating agent, Thermochim. Acta 444 (2006) 201–205.
[67] D. Wood, N. Bubb, A. Clifford, R. Hill, J. Knowles, An investigation into the crystallization of Dicor glass–ceramic, J. Mater. Sci. Lett. 18 (1999) 1001–1002.
[68] K. Kodaira, H. Fukuda, S. Shimada, T. Matsushita, A. Tsunashima, Preparation and characterization of fluorphlogopite-fluormuscovite mica glass-ceramics, Mater. Res. Bull. 19 (1984) 1427–1432.
[69] M.D. Glendenning, W.E. Lee, Microstructural development on crystallizing hot-pressed pellets of cordierite melt-derived glass containing B2O3 and P2O5, J. Am. Ceram. Soc. 79 (1996) 705–713.
[70] H. Elhaes, M. Attallah, Y. Elbashar, A. Al-Alousi, M. El-Okr, M. Ibrahim, Modeling and optical properties of P2O5–ZnO–CaO–Na2O glasses doped with copper oxide, J. Comput. Theor. Nanosci. 11 (2014) 2079–2084.
[71] V. Klyuev, A. Mal'shikov, Synthesis and properties of SiO2–P2O5 glasses, Fiz. Khim. Stekla 15 (1989) 746–749.
[72] J. Wu, C. Lin, J. Liu, L. Han, H. Gui, C. Li, T. Liu, A. Lu, The effect of complex nucleating agent on the crystallization, phase formation and performances in lithium aluminum silicate (LAS) glasses, J. Non-Cryst. Solids 521 (2019), 119486.